frontiers | Frontiers in Materials

TYPE Original Research
PUBLISHED 19 December 2022
DOI 10.3389/fmats.2022.1098304

OPEN ACCESS

EDITED BY
Li Li,
Northwest A&F University, China

REVIEWED BY
Erol Yilmaz,
Recep Tayyip Erdoğan University, Turkey
Shaker Qaidi,
University of Duhok, Iraq

*CORRESPONDENCE
Kaffayatullah Khan,
kkhan@kfu.edu.sa

SPECIALTY SECTION
This article was submitted to Structural Materials, a section of the journal Frontiers in Materials

RECEIVED 14 November 2022
ACCEPTED 05 December 2022
PUBLISHED 19 December 2022

CITATION
Khan K, Amin MN, Sahar UU, Ahmad W, Shah K and Mohamed A (2022), Machine learning techniques to evaluate the ultrasonic pulse velocity of hybrid fiber-reinforced concrete modified with nano-silica.
Front. Mater. 9:1098304.
doi: 10.3389/fmats.2022.1098304

Machine learning techniques to evaluate the ultrasonic pulse velocity of hybrid fiber-reinforced concrete modified with nano-silica

Kaffayatullah Khan[1]*, Muhammad Nasir Amin[1], Umbreen Us Sahar[2], Waqas Ahmad[3], Kamran Shah[4] and Abdullah Mohamed[5]

[1]Department of Civil and Environmental Engineering, College of Engineering, King Faisal University, Al-Ahsa, Saudi Arabia, [2]Civil Engineering Department, University of Engineering and Technology, Lahore, Pakistan, [3]Department of Civil Engineering, COMSATS University Islamabad, Abbottabad, Pakistan, [4]Department of Mechanical Engineering, College of Engineering, King Faisal University, Al-Ahsa, Saudi Arabia, [5]Research Centre, Future University in Egypt, New Cairo, Egypt

It is evident that preparing materials, casting samples, curing, and testing all need time and money. The construction sector will benefit if these problems can be handled using cutting-edge techniques like machine learning. Also, a material's ultrasonic pulse velocity (UPV) is affected by various variables, and it is difficult to study their combined effect experimentally. This research used machine learning to assess the UPV and SHapley Additive ExPlanations techniques to study the impact of input parameters of hybrid fiber-reinforced concrete modified with nano-silica (HFRNSC). Three ML algorithms were employed, i.e., gradient boosting regressor, adaptive boosting regressor, and extreme gradient boosting, for ultrasonic pulse velocity evaluation. The accuracy of machine learning models was measured *via* the coefficient of determination (R^2), k-fold analysis, statistical tests, and comparing the predicted and actual ultrasonic pulse velocity. This study determined that the gradient boosting and adaptive boosting models had a good level of accuracy for ultrasonic pulse velocity, but the extreme gradient boosting method estimated the ultrasonic pulse velocity of HFRNSCs with a greater degree of precision. Also, from the statistical checks and k-fold approach, it was discovered that the extreme gradient boosting method is more exact in estimating the ultrasonic pulse velocity of HFRNSCs. The SHapley Additive ExPlanations analysis revealed that the age of the specimen and nano-silica had a greater positive impact on the ultrasonic pulse velocity of HFRNSCs, whereas the coarse aggregate to fine aggregate ratio had a negative impact. In addition, fiber volume was found to have both positive and negative effects. By aiding the development of rapid and low-cost methods for determining material properties and the influence of input parameters, the construction industry may profit from the use of such technologies.

KEYWORDS

nano-silica, fiber-reinforced concrete, ultrasonic pulse velocity, machine learning, SHAP analysis, hybrid fibers

1 Introduction

Concrete is a commonly used building material (AMIN et al., 2019; KHAN et al., 2022F; KHAN et al., 2022G). To lower the brittleness of concrete, scholars are investigating fiber-reinforced concrete (FRC), which is significantly more ductile than conventional concrete (KHAN et al., 2018; LI AND DENG, 2021; XIE et al., 2021; ZAID et al., 2021). The onset of concrete failure is the emergence of cracks (CAO et al., 2019; XUPENG et al., 2021). The introduction of hybrid FRC, which is comprised of multiple fibers (glass, steel, and polypropylene), is proposed to enhance the mechanical performance and energy absorption capacity of concrete (CAO et al., 2018A; HUANG et al., 2021; XUE AND YILMAZ, 2022; ZHAO et al., 2022). Fibers restrict the growth of cracks in concrete, thereby allowing structural elements to withstand greater deformations following the development of early cracks (cao et al., 2018B; ABIRAMI et al., 2020; CHUN et al., 2022; ZHANG et al., 2022). Nanoparticles, such as nano-silica (NS), have been shown to fill holes in cement paste and improve the mechanical performance and durability of concrete (BAHARI et al., 2016; CAO et al., 2020; MURAD, 2021; KHAN et al., 2022E). Consequently, using nanoparticles in FRC might result in a material with enhanced performance that is perfect for constructing durable, high-performance structures (HAO et al., 2021). NS decreases the setting time of the mix and increases its early-age strength. A crucial characteristic of NS is its nanostructure, which offers an exceptionally greater specific surface area (SSA) and thus works as an aggregate-cement binder (WANG et al., 2018). The strong pozzolanic effect of NS is due to its nanoparticle size (ARDALAN et al., 2017; YING et al., 2017). The interfacial transition zone (ITZ), which is considered a weak region in concrete, is also strengthened because these nanoparticles cover all gaps and voids, hence decreasing permeability (XU et al., 2017; SHARKAWI et al., 2018). NS is a highly effective ingredient for accelerating the hydration and producing more calcium-silicate-hydrate (C-S-H) gel in concrete, which is responsible for the achievement of concrete strength (NIEWIADOMSKI et al., 2017; NORHASRI et al., 2017; MOHAMMED et al., 2018; REN et al., 2018; ZAHIRI AND ESKANDARI-NADDAF, 2019). In cementitious materials, the quantity of portlandite-$Ca(OH)_2$ reduces when NS and $Ca(OH)_2$ combine to form a denser product (MASSANA et al., 2018). Certain prior research suggests that replacing NS for up to 4% of the cement can improve the material's durability and strength under adverse conditions like corrosion and high temperatures (ERDEM et al., 2018; MAHAPATRA AND BARAI, 2019). The excessive quantity of NS might cause particle aggregation due to non-uniform dispersal, thus reducing workability (ZAREEI et al., 2019). To improve the macroscopic characteristics and performance of cementitious composites, several nanoparticles are utilized as additives, and NS has become frequent among these nanoparticles. Notwithstanding, the limited practical applications of NS in the building industry are a result of their higher costs, which are approximately 1,000 times more expensive than ordinary cement (RECHES, 2018; FANG et al., 2021).

From the standpoint of evaluating the structural health of concrete structures, ultrasonic pulse velocity (UPV) has been identified as an essential measure (BOLBOREA et al., 2021; KARIMAEI et al., 2021). Numerous research was conducted to comprehend the correlation between UPV and concrete compressive strength (YAN et al., 2021; ZHANG AND ASLANI, 2021). Similarly to compressive strength, the UPV of concrete likewise increases with age and is inversely related to the pore volume in the matrix (KOU et al., 2012). The rate of change of UPV with time may be utilized not only to estimate the setting of a mix but also to show distinct phases of microstructural changes in the matrix (LATIF AL-MUFTI AND FRIED, 2012; BARLUENGA et al., 2015). It was also shown that UPV is impacted by microstructural differences in the mortar and may be utilized to efficiently assess sand concentration in a mortar (MOLERO et al., 2009). Additionally, the UPV of concrete was explored to identify deterioration within the concrete (OULD NAFFA et al., 2002; LENCIS et al., 2021).

In two ways, the UPV test findings of FRC vary from those of plain concrete. Firstly, since the observed velocity is directly related to the concentration of the medium through which it is propagated, the insertion of different fibers might vary the density of the concrete and, therefore, the UPV findings (ASHRAFIAN et al., 2018). For instance, recent studies observed that the UPV of steel FRC was higher than the plain concrete; however, the UPV of FRC with low-density fibers, like polyphenylene sulfide or recycled polyethylene terephthalate, was less than plain concrete (RAHMANI et al., 2013; SADEGHI NIK AND LOTFI OMRAN, 2013). Secondly, the introduction of varying amounts of fibers might affect the concrete's compaction level and, subsequently, its porosity (LI et al., 2022A; QIN et al., 2022; ZHENG et al., 2022). Previously, it was demonstrated that the slightly increased porosity of concrete resulting from the integration of 1% fibers by volume reduced the UPV of FRC samples, including polypropylene and steel fibers, by 4% and 3%, respectively (SUKONTASUKKUL et al., 2010). The number of parameters impacting concrete and the length of time necessary to establish the characteristics of hardened concrete motivate the search for alternate estimation techniques. UPV, which relies on ultrasonic wave speed transmission through the matrix, has been used to determine

the characteristics of hardened concrete (TRTNIK et al., 2009; HUANG et al., 2011; DÜĞENCI et al., 2015; MOBINI et al., 2015). As previously demonstrated, the UPV of concrete mixes is an excellent indicator of their mechanical characteristics, including compressive and flexural strength and modulus of elasticity (TRTNIK et al., 2009). Large, thin, and difficult-to-access elements make it difficult to assess the UPV of the concrete. Not only do data-driven models assist minimize the time and expense of testing by supplying designers with vital data, but they also aid in avoiding complications that emerge during the assessment of the many hardened characteristics of FRC. The progress of innovative formula-based models with high precision to forecast this essential attribute can greatly minimize concrete waste by reducing the number of trial mixes necessary to get the ideal blend (KHAN et al., 2022H). Artificial intelligence-based practices, like machine learning (ML), are among the highly modern prediction procedures used in the present issue area (NAFEES et al., 2021; KHAN et al., 2022A; NAFEES et al., 2022A; NAFEES et al., 2022B; ILYAS et al., 2022). These methods imitate results based on the input dataset, and resultant models are validated by testing. The utilization of ML techniques to anticipate the characteristics of construction materials is gaining prominence (SHAFABAKHSH et al., 2015; AWOYERA et al., 2020; KHAN et al., 2022D). The most of past ML-based researches centered on estimating the strength of traditional concrete (QI et al., 2022; SHAH et al., 2022; SHARMA et al., 2022), while few research has been published on predicting the UPV of FRC. Therefore, it is vital to study the effectiveness of ML methods in estimating the UPV of FRC.

This research utilized the data sample to estimate the UPV of hybrid fiber-reinforced concrete modified with NS, hereinafter called HFRNSC, by employing ML methods. Three ML methods from boosting family were employed, i.e., gradient boosting regressor (GBR), Adaptive boosting regressor (ABR), and extreme gradient boosting (XGB), to achieve the study's aims. Coefficient of determination (R^2), k-fold technique, statistical tests, and comparing estimated and actual results were used to assess and evaluate the performance of each model. It is obvious that conducting experiments requires a great deal of time, money, and effort due to the necessity of gathering materials, casting samples, curing, and testing. These issues might be resolved using cutting-edge methods like ML, which will be a benefit for the building industry. Moreover, the UPV and strength of HFRNSCs depend on a number of factors, and it is challenging to measure their combined influence using experimental methods. The influencing factors include fiber volume (Vf), coarse aggregate to fine aggregate ratio (CA/FA), superplasticizer to binder ratio (SP/B), water to binder ratio (w/b), NS, and age of specimen ((A). To investigate the relationship between the input characteristics and the UPV of HFRNSCs, a SHapley Additive exExplanations (SHAP) analysis was conducted. The literature may be mined for a data sample to use with ML methods. As a result, the information gathered may be used to run ML methods, estimate material characteristics, and evaluate the influence of input factors. In this work, a dataset was used to evaluate the performance of several ML methods for predicting the UPV of HFRNSCs and to determine the relative importance of various input variables in producing accurate predictions.

2 Materials and methods

In order to get desired findings, ML methods require a wide collection of input variables (SUFIAN et al., 2021). For this purpose, a literature search was performed using six input parameters, including Vf, CA/FA, w/b, NS, SP/B, and the age of the specimen. To avoid bias, data samples were collected arbitrarily from previous studies (SADRMOMTAZI AND FASIHI, 2010; ASHRAFIAN et al., 2018), and data points containing UPV results were collected for algorithm execution. In this research, 132 data samples were recorded from the literature and employed to train ML techniques. The combination's proportions and the desired outcome were considered when obtaining the data since models called for similar input variables for each mixture to estimate the required results. Three types of fiber, including glass, steel, and polypropylene, were used in the samples as hybrid fibers. The length and diameter of steel fibers were 36 mm and 0.7 mm, respectively, while the length and diameter of polypropylene and glass fibers were 12 mm and 0.1 mm, respectively. For the ML algorithms to run, all six features were used as inputs, with UPV serving as the result. The statistical details of inputs and outcomes are summarized in Table 1. The standard deviation, maximum, and minimum, show the range of values, whereas the mode, mean, and median show the basic tendencies.

The UPV of HFRNSCs was analyzed by employing published research data. The goals of the study were attained by employing ML strategies using *Python* code and Spyder (version 5.1.5) tool from the Anaconda Navigator software. The UPV of HFRNSCs was evaluated using GBR, ABR, and XGB ML techniques. In practice, these ML techniques are typically employed to approximate outputs from given inputs (YUAN et al., 2022). ML techniques are being employed to predict the strength, durability, and temperature resistance of materials (AMIN et al., 2022; KHAN et al., 2022C). Nevertheless, there are some limitations associated with the use of ML methods. Specifically, challenges associated with dataset generation, model validation, and model deployment, as reported by (LI et al., 2022B). The allocation of testing and training data samples utilized for the model was 30% and 70%, respectively. The precision of a model may be noted from the R^2 value of the predicted result. Values closer to zero imply more variance, whereas values closer to one indicate that the prediction model and experimental findings are nearly completely matched (AHMAD et al., 2022). The k-fold method and statistical measures, including mean absolute error (MAE),

TABLE 1 Statistical parameters of input and output parameters.

Parameter	Vf (%)	CA/FA	W/b	NS (kg/m^3)	SP/B	Age (days)	UPV (km/s)
Mean	0.23	0.88	0.39	23.95	0.02	40.76	5.23
Standard Error	0.02	0.00	0.00	1.61	0.00	3.00	0.02
Median	0.20	0.87	0.39	24.00	0.02	28.00	5.23
Mode	0.20	0.87	0.39	0.00	0.02	7.00	5.15
Standard Deviation	0.20	0.01	0.01	18.50	0.00	34.48	0.22
Minimum	0.00	0.87	0.39	0.00	0.02	7.00	4.49
Maximum	0.90	0.91	0.43	49.60	0.03	90.00	5.61

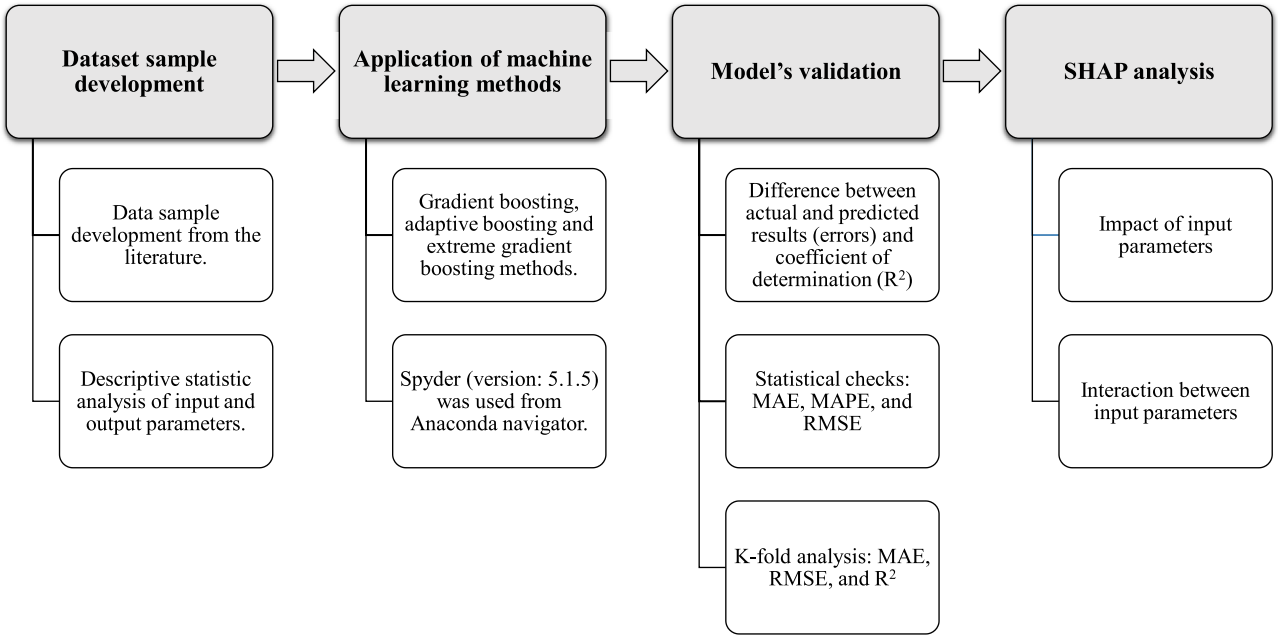

FIGURE 1
Flowchart of research methods.

root mean squared error (RMSE) and mean absolute percentage error (MAPE), were employed to measure the exactness of a model. The sequence of study methods is shown in Figure 1. The subsequent sub-sections elaborate on the ML techniques and validation strategies that were put to use in this study.

2.1 Gradient boosting regressor (GBR)

The GBR ensemble method of regression and classification was first proposed by FRIEDMAN (2001). GBR is similar to other boosting techniques, except it can only be used for regression. As can be seen in Figure 2, the strategy randomly selects repetitions from the training set and then verifies them using the base model. As a result, preventing overfitting may be achieved by arbitrarily subsampling the training data sample, which can increase GBR's accuracy and speed. The rate of regression to fit tends to increase as the sample size of the training data decreases. Tuning factors for GBR include the shrinkage rate and n-trees, where n-trees is the total number of trees produced. In this case, n trees are not a small enough number; therefore, the learning rate (shrinkage factor) is applied to each expansion tree individually.

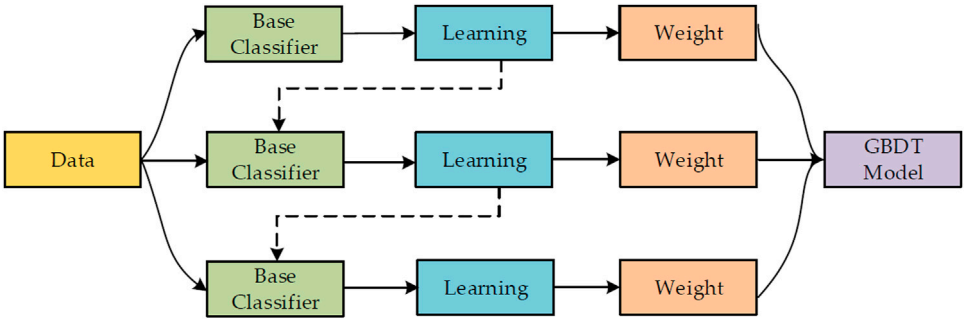

FIGURE 2
Structure of GBR training method (YAO et al., 2019).

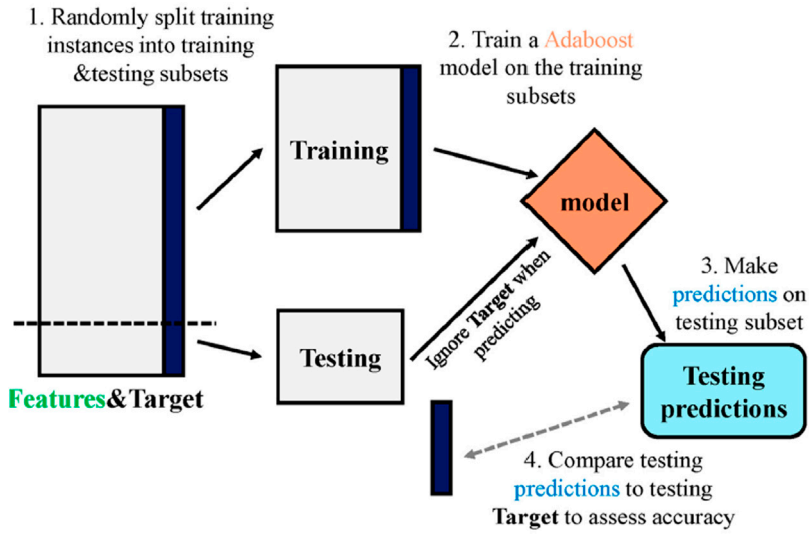

FIGURE 3
Structure of ABR training method (WANG et al., 2021).

2.2 Adaptive boosting regressor (ABR)

Figure 3 depicts the procedure for making an ABR-based estimation. The term "multi-classifiers" refers to the ensemble that is created when many algorithms are combined. An educational community of about a thousand people working together to find a solution to the situation. Ensemble learning, effectively a supervised ML methodology, is one way to tackle ABR. In adaptive boosting, weights are linked to each occurrence, with greater weights attached to examples that were incorrectly categorized. It is common practice in supervised machine learning to employ boosting algorithms in order to mitigate bias and reduce variance. Assisting struggling pupils through the use of ensemble strategies. It takes in as many decision trees as you like during the training process. Incorrectly classified data inside the core model are revealed during the decision tree building phase. Another model uses the same set of data records as inputs. This process would continue until enough number of novice learners were produced. For problems involving binary classification, ABR facilitates the growth of the decision tree's operational capabilities. It's also used to make the ML model more efficient. It's a great tool for those who study slowly. These ensemble methods see extensive use in the field of materials science, particularly in the estimation of concrete's mechanical properties (YANG et al., 2022).

2.3 Extreme gradient boosting (XGB)

The XGB technique was developed by CHEN AND GUESTRIN (2016) and is regarded as a trustworthy tool for

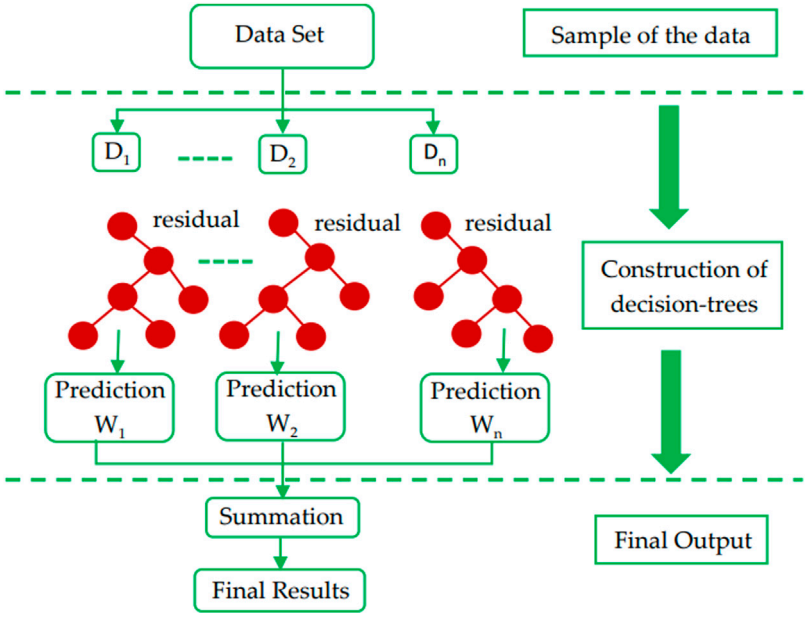

FIGURE 4
Schematic illustration of XGB procedure (AMJAD et al., 2022).

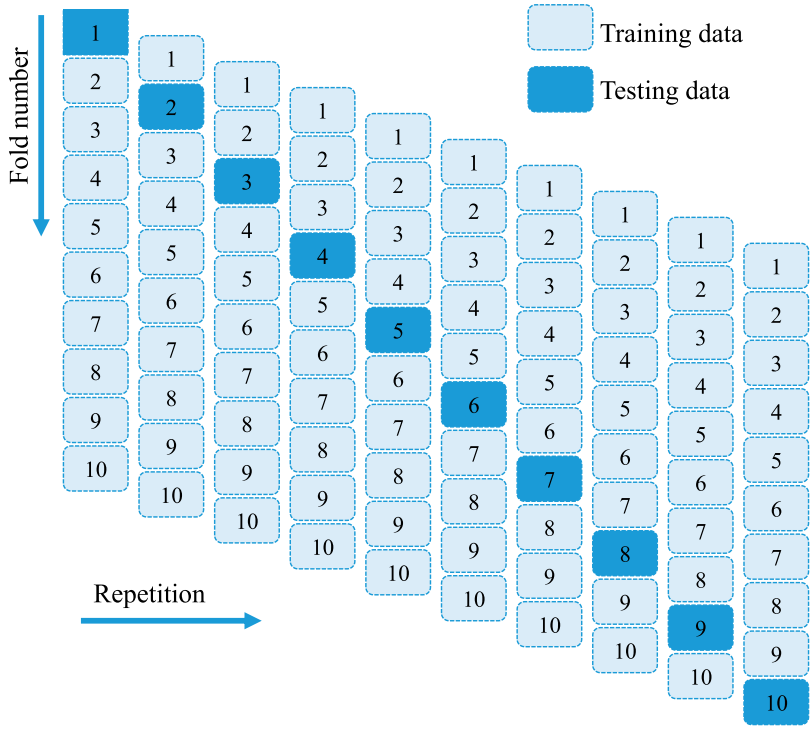

FIGURE 5
K-fold validation process.

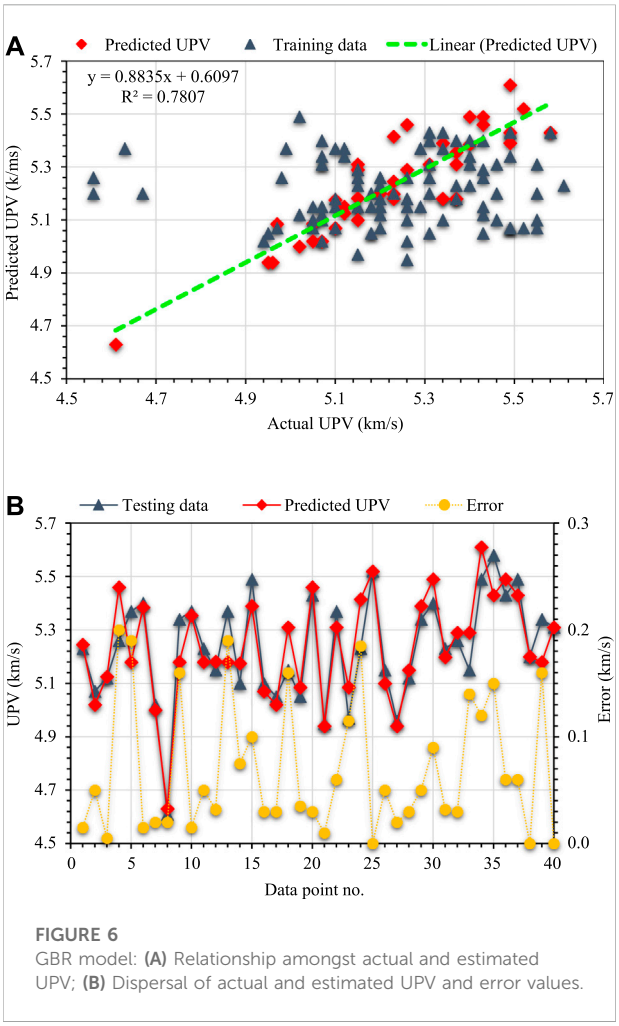

FIGURE 6
GBR model: **(A)** Relationship amongst actual and estimated UPV; **(B)** Dispersal of actual and estimated UPV and error values.

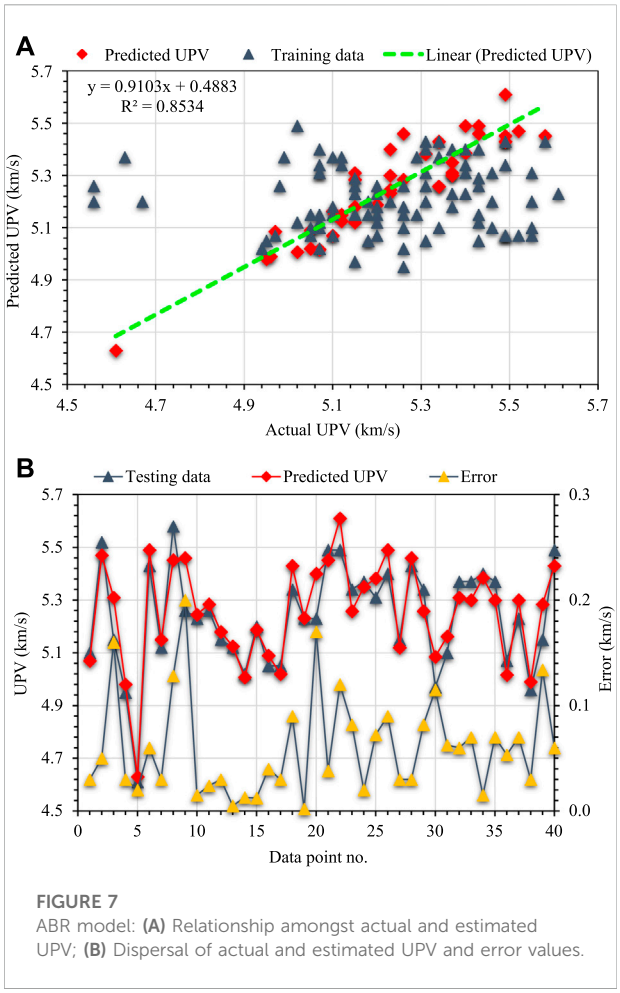

FIGURE 7
ABR model: **(A)** Relationship amongst actual and estimated UPV; **(B)** Dispersal of actual and estimated UPV and error values.

data science scholars since it uses a tree-based ensemble learning approach. XGB is built on the GBR architecture, which involves using several functions to estimate outcomes according to Eq. 1 (FRIEDMAN, 2001).

$$\bar{y}_i = y_i^0 + \eta \sum_{K=1}^{n} f_k(U_i). \quad (1)$$

The anticipated output is represented by $\bar{y}_i$ with i^{th} data and $\mathbf{U_i}$ as the variable vector; η represents the estimator quantity in connection with separate tree structures next to each $\mathbf{f_k}$ With k ranging from 1 to n; and $\mathbf{y_i^0}$ is the null hypothesis represents the learning rate to improve the accuracy of the model, as well as the connection of new trees to prevent overfitting. Building a model with minimum overfitting is a significant difficulty in ML. The training phase of the XGB model is assessed in a complementary manner.

According to Eq. 1, at the k^{th} level, the k^{th} predictor is associated with the model and the prediction of k^{th} $\mathbf{y_i^{-k}}$ is calculated using the expected output $\mathbf{y_i^{-(k-1)}}$, with the respective produced f_k against the k^{th} corresponding predictor supplied in Eq. 2.

$$y_i^{-k} = y_i^{-(k-1)} + \eta f_k \quad (2)$$

Where f_k is leave's weight formed by minimizing the k^{th} tree factual task Eq. 3.

$$f_{obj} = \gamma Z + \sum_{a=1}^{Z} \left[g_a \omega_a + \frac{1}{2} (h_a + \lambda) \omega_a^2 \right] \quad (3)$$

Where leaf node fraction is indicated by Z, complexity factor by $\boldsymbol{\gamma}$, constant coefficient by $\boldsymbol{\lambda}$, and leaf weight by $\boldsymbol{\omega_a^2}$, $\boldsymbol{\lambda}$ and $\boldsymbol{\gamma}$ are controlling parameters used to prevent overfitting and enhance the model. $\mathbf{h_a}$ and $\mathbf{g_a}$ are the summation factors for the whole data sample associated with the prior and initial gradient leaf loss functions, respectively. For the construction of the k^{th} tree, a leaf is divided into many leaves. Such a system is implemented using gain parameters, as shown in Eq. 4.

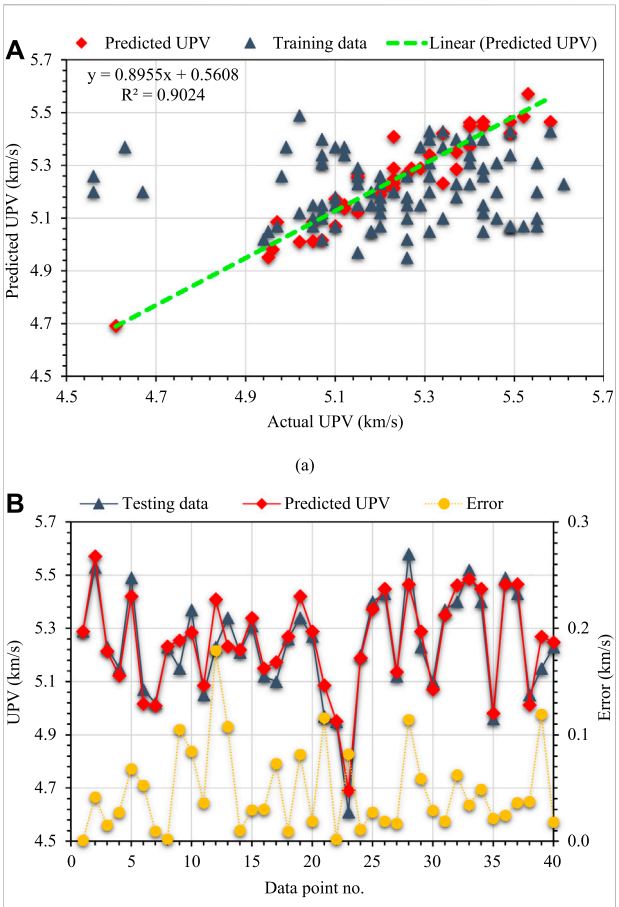

FIGURE 8
XGB model: **(A)** Relationship amongst actual and estimated UPV; **(B)** Dispersal of actual and estimated UPV and error values.

TABLE 2 Error assessments of the build ML-based models using statistical tests.

Model	MAE (km/s)	MAPE (%)	RMSE (km/s)
GBR	0.070	1.30	0.093
ABR	0.061	1.20	0.077
XGB	0.047	0.90	0.062

$$G = \frac{1}{2}\left[\frac{O_L^2}{P_L + \lambda} + \frac{O_R^2}{P_R + \lambda} + \frac{(O_L + O_R)^2}{P_L + P_R + \lambda}\right] \quad (4)$$

Where gain parameters are represented by **G**, the right and left leaves are designated by $\mathbf{P_R}$ and $\mathbf{O_R}$ and $\mathbf{P_L}$ & $\mathbf{O_L}$, respectively. In general, the division criterion is assumed while the approximation of the gain parameter to zero. $\boldsymbol{\lambda}$ is a regulating variable that is indirectly reliant on gain settings. For instance, a bigger regularization value might significantly reduce the gain parameter, hence stopping the leaf convolution process. However, the performance of the model when incorporating training data would also be diminished. Figure 4 depicts the fundamental level-wise structure of the XGB tree model.

2.4 Validation of models

The ML algorithms were verified using statistical tests and k-fold approaches. The k-fold technique is commonly used to assess a model's performance by randomly dividing samples of relevant data into 10 groups (AHMAD et al., 2021). Figure 5 illustrates how nine classes are utilized to train ML models, whereas just one is used for testing. The ML method performs better when errors are lower, and R^2 is higher. In addition, this approach needs to be repeated 10 times, which results in the model's exceptional accuracy. Errors assessment (MAE, RMSE, and MAPE) was also used statistically to assess the accuracy of each ML method. Statistical analysis was performed on the projections made by the ML approaches using Eqs 5–7, which were obtained from prior work (ASLAM et al., 2020; FAROOQ et al., 2021).

$$MAE = \frac{1}{n}\sum_{i=1}^{n}|P_i - Ti| \quad (5)$$

$$RMSE = \sqrt{\sum \frac{(P_i - T_i)^2}{n}} \quad (6)$$

$$MAPE = \frac{100\%}{n}\sum_{i=1}^{n}\frac{|P_i - Ti|}{T_i} \quad (7)$$

where n = number of data points, P_i = predicted findings, and T_i = actual results.

3 Results and analysis

3.1 GBR model

Figure 6 shows the outcomes of the GBR model for estimating the HFRNSC's UPV. Figure 6A displays the relation among actual and estimated UPV. The GBR approach estimated UPV with a moderate level of accuracy and divergence among actual and estimated findings. The R^2 of 0.78 suggests that the GBR method for calculating the UPV of HFRNSCs is satisfactory, and the actual and estimated results reasonably agree. Figure 6B presents the actual, estimated, and error values distribution for the GBR model. The error values varied up to 0.200 km/s, with a mean of 0.070 km/s. Additionally, the percentage variance of errors was evaluated, and it was found that 47.5% of the error readings were lower than 0.05 km/s, 22.5% fell among 0.05–0.1 km/s, and 30.0% were higher than 0.1 km/s. The analysis of errors indicated that the GBR strategy estimated the UPV of HFRNSCs reasonably.

TABLE 3 K-fold analysis results.

Fold no.	GBR			ABR			XGB		
	MAE (km/s)	RMSE (km/s)	R^2	MAE (km/s)	RMSE (km/s)	R^2	MAE (km/s)	RMSE (km/s)	R^2
1	0.09	0.10	0.74	0.08	0.11	0.72	0.07	0.07	0.76
2	0.07	0.09	0.63	0.06	0.09	0.63	0.08	0.07	0.82
3	0.11	0.12	0.61	0.09	0.12	0.58	0.09	0.08	0.71
4	0.09	0.11	0.57	0.08	0.10	0.65	0.08	0.10	0.90
5	0.10	0.08	0.72	0.10	0.08	0.78	0.05	0.07	0.83
6	0.09	0.09	0.64	0.08	0.08	0.81	0.05	0.07	0.85
7	0.07	0.19	0.73	0.07	0.09	0.84	0.07	0.11	0.86
8	0.18	0.29	0.32	0.06	0.15	0.76	0.09	0.17	0.39
9	0.07	0.14	0.78	0.07	0.22	0.85	0.06	0.06	0.88
10	0.16	0.19	0.45	0.08	0.13	0.33	0.05	0.18	0.52

3.2 ABR model

Figure 7 presents the findings of the ABR model in forecasting the UPV of the HFRNSCs. The relation amongst actual and forecasted UPV is seen in Figure 7A. In comparison with the GBR approach, the ABR technique produced more accurate results and the minimum difference among actual and estimated findings. Compared to other models, the ABR model is more precise, as seen by its R^2 score of 0.85. The distribution of real, estimated, and error values generated by the ABR approach are depicted in Figure 7B. The lowest error was 0.002 km/s, the mean error was 0.061 km/s, and the highest error was 0.200 km/s. The distribution of error values was: 47.5% were below 0.05 km/s, 35.0% were between 0.05 and 0.1 km/s, and 17.5% were over 0.1 km/s. Since the ABR model had a smaller deviation of errors, it was concluded that it was more accurate than the GBR model. Due to the usage of an endless number of decision trees during training and its initial decision tree's emphasis on incorrectly categorized input, the ABR model achieves better accuracy. Another model also makes use of the same data. This process is repeated until enough number of basic learners have been created. Additionally, ABR improves the effectiveness of decision trees for classifying data into two categories.

3.3 XGB model

Figure 8 exhibits the results of the XGB method to foretell the UPV of HFRNSCs. A connection among actual and forecasted UPV is shown in Figure 8A. The XGB method produced the fewest discrepancies amongst real and anticipated data as compared to the other models used. The higher R^2 of 0.90 for the XGB model reflects its improved accuracy. The XGB method's actual, estimated, and errors are shown in Figure 8B. The average error was calculated to be 0.047 km/s, while the maximum error was calculated to be 0.179 km/s. Nearly 65.0% of the errors were found to be less than 0.05 km/s, 20.0% were found to be between 0.05 and 0.1 km/s, and 15.0% were found to be larger than 0.1 km/s. The error distribution showed that the XGB model was more accurate than the GBR and ABR models. But the accuracy of the other models used is equally satisfactory. The XGB model is more precise because it employs a tree-based ensemble learning strategy that optimizes output by generating submodels.

3.4 Model's validation

Table 2 displays the results of the error evaluations (MAE, RMSE, and MAPE) utilizing the aforementioned Eqs.s 5-7 for UPV estimation models. The MAE for predicting UPVs were found to be 0.070 km/s for GBR, 0.061 km/s for ABR, and 0.047 km/s for XGB. According to the calculations, the MAPE for GBR was 1.30%, ABR was 1.20%, and XGB was 0.90%. In addition, it was found that the RMSE for GBR, ABR, and XGB were 0.093, 0.077, and 0.062 km/s, respectively. These evaluations also showed that the XGB method had a lower error rate than the GBR and the ABR, making it more exact. Table 3 displays the results of calculating the k-fold method's validity using R^2, RMSE, and MAE. The k-fold analysis for the UPV prediction was compared using the various ML approaches used, and the results are depicted in Figure 9, Figure 10, and Figure 11. The MAE for the UPV estimation using the GBR method ranged from 0.07 to 0.18 km/s, with a mean of 0.10 km/s. The MAE for the ABR model was 0.06–0.10 km/s, with an average of 0.08 km/s. The XGB model had an MAE

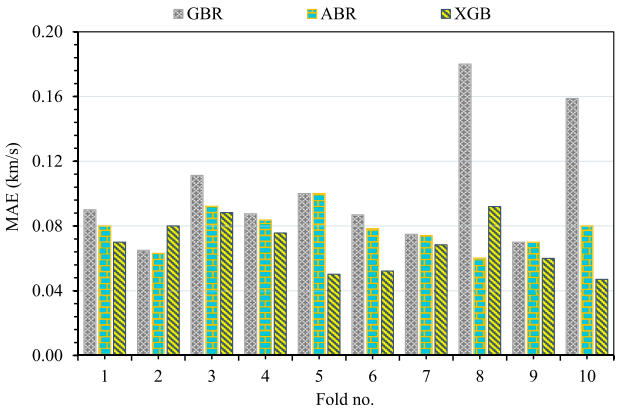

FIGURE 9
MAE values for all models from the k-fold analysis.

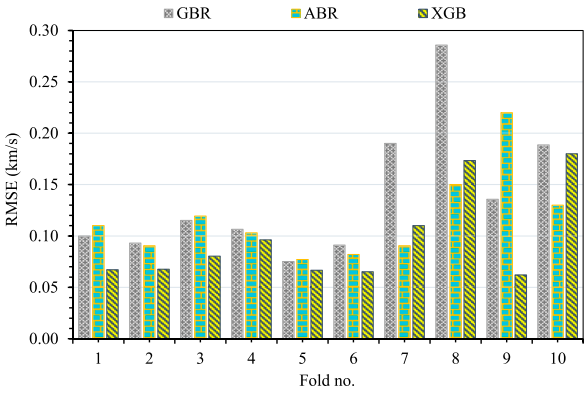

FIGURE 10
RMSE values for all models from the k-fold analysis.

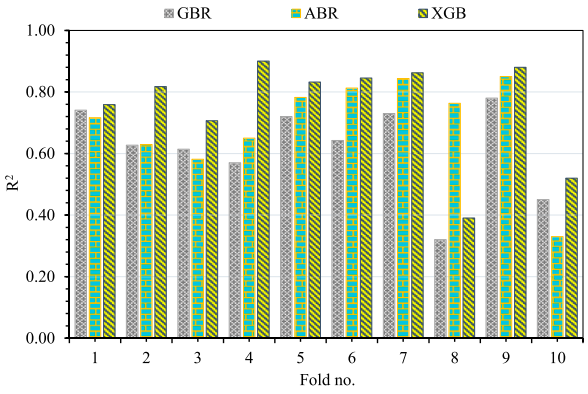

FIGURE 11
R^2 values for all models from the k-fold analysis.

distribution from 0.05 to 0.09 km/s, with an average of 0.07 km/s. Similar results were found when comparing the RMSE of the GBR, ABR, and XGB methods. The average RMSE for GBR, ABR, and XGB was 0.14, 0.12, and 0.10 km/s, respectively. However, the average R^2 values for GBR, ABR, and XGB were 0.62, 0.70, and 0.75, respectively. The XGB model predicted the UPV of HFRNSCs with the fewest errors, and the highest R^2 was the most reliable. However, both the ABR and GBR models achieved reasonable levels of accuracy. Therefore, all of the models might be used to precisely evaluate the UPV of HFRNSCs.

3.5 Impact of input features on UPV

This study looked at how different input characteristics affected the UPV of HFRNSCs. SHAP tree explainer is used across the board to include local SHAP explanations into a more comprehensive narrative of global feature impacts. Input-by-input, the violin SHAP plot shows how HFRNSCs' UPV responds to all stimuli (see Figure 12). The *x*-axis represents the final SHAP value after all parameters have been adjusted, and the *y*-axis represents the contribution of each individual parameter. The positive correlation among the age of specimen A) and UPV of HFRNSCs was bigger than that of any other characteristic (more red points on the positive side). It was determined that UPV rises as specimen age A) rise. It was also demonstrated that the impact of NS on the UPV was more positive. It might be because NS acts as a filler, decreasing the porosity of the matrix and leading to an increase in UPV. In contrast, it was shown that CA/FA had a larger negative effect on UPV, suggesting that CA/FA should be kept low to get a higher UPV. One probable explanation is that UPV is inversely

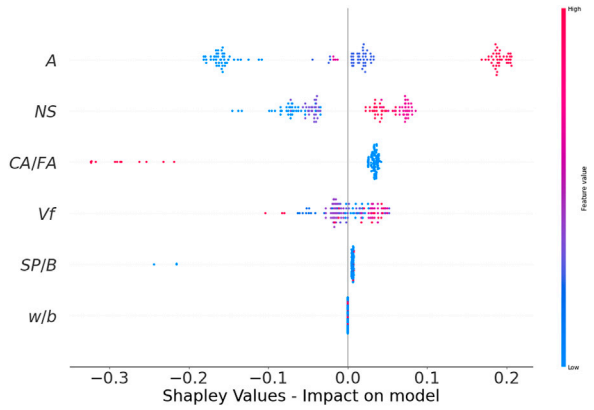

FIGURE 12
SHAP plot signifying the effect of input features on UPV.

proportional to matrix porosity (MOHAMMED AND RAHMAN, 2016); thus, when CA/FA increases, UPV decreases. It was shown that Vf had both positive and negative effects, suggesting that utilizing Vf up to an optimal amount can improve the UPV but that at larger Vf concentrations, the UPV would decrease. The impact of SP/B and w/b could not be determined due to the absence of input value variation in the used dataset. Using a bigger data sample with more varied input features can better interpret their impact.

Figure 13 displays the relation amongst prominent input parameters and their effect on the UPV of HFRNSCs. Figure 13A shows the interaction of specimen age A). The plot demonstrates that as the specimen age A) increases, the UPV rises and mainly interacts with the NS. It can be established that with increasing age, the reaction between NS and $Ca(OH)_2$ takes place, resulting in the formation of dense microstructure, increasing the UPV of the sample. Likewise, incorporating NS in FRC has a favorable effect on UPV (Figure 13B) and interacts mostly with specimen age A). However, utilizing NS up to the optimal quantity will help improve the UPV of HFRNSCs. Hence, NS may be employed in the range of 30–40 kg/m^3 to achieve higher UPV. Furthermore, as depicted in Figure 13C, increasing CA/FA has a detrimental effect on UPV. Therefore, the CA/FA should be maintained lower to get a higher UPV. The UPV of the HFRNSC is also affected by Vf, as shown in Figure 13D. UPV rises with Vf concentration up to 0.5%, then drops and largely interacts with the NS. For getting a high UPV for HFRNSC under these

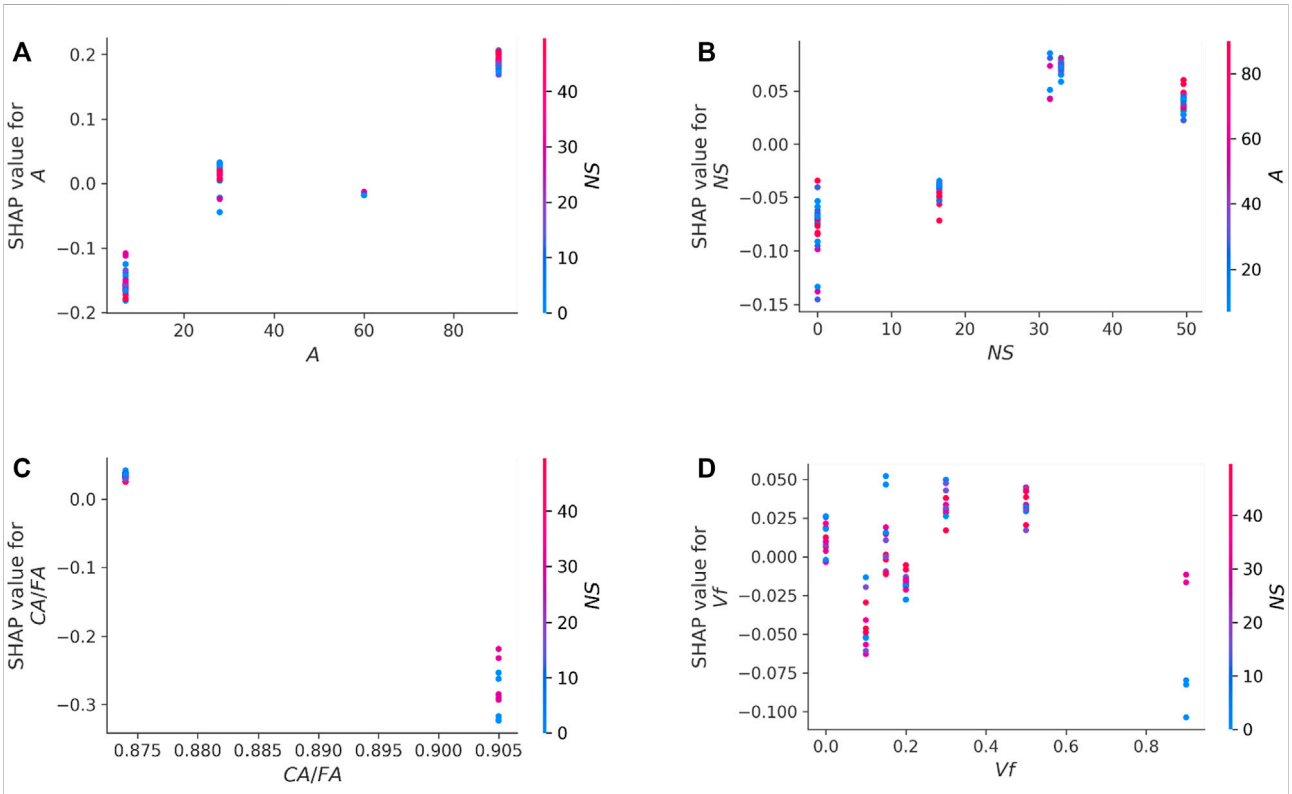

FIGURE 13
Interaction of input parameters and their impact on UPV: **(A)** Age of specimen; **(B)** Nano-silica; **(C)** Coarse aggregate to fine aggregate ratio; **(D)** Fiber volume.

FIGURE 14
Distribution of R^2 for the XGB UPV and FS models.

TABLE 4 Best ML techniques recommended in past studies.

Study	Material studied	Properties predicted	ML method used	Best ML technique reported
ZHENG et al. (2022)	Steel fiber -reinforced concrete	Flexural strength	GBR, random forest, and XGB	XGB
KHAN et al. (2022b)	Geopolymer concrete	Compressive strength	Support vector machine, GBR, and XGB	XGB
WANG et al. (2022)	Geopolymer concrete	Compressive strength	Decision tree, ABR, and random forest	ABR
SHANG et al. (2022)	Recycled aggregate concrete	Compressive and split-tensile strength	Decision tree and ABR	ABR
AL-HASHEM et al. (2022)	Steel fiber-reinforced concrete	Compressive and flexural strength	Multiple-layer perceptron neural network and ABR	ABR
ANJUM et al. (2022)	Fiber reinforced concrete	Compressive strength	Bagging, random forest, GBR, and ABR	ABR

circumstances while employing the same components as in the current study, a Vf of almost 0.5% is ideal. These findings heavily rely on the nature of the inputs used and the scope of the dataset used in this analysis. Depending on the parameters and data used, the results may change.

4 Discussions

In this study, GBR, ABR, and XGB ML methods were utilized to evaluate the HFRNSCs' UPV. Each method was tested for precision to determine which one was the most reliable indicator. The XGB approach yielded more precise findings, with an R^2 of 0.90, for UPV prediction than the GBR and ABR methods, which had R^2 of 0.78 and 0.85, respectively. The error readings provided additional proof of the XGB method's better accuracy. The error analysis reveals that the XGB models had a better agreement between real and estimated values than the GBR and ABR methods. Table 4 is generated to compare the optimum ML methods of the present study with the literature. Previous studies have proven the XGB method's superior accuracy in forecasting the strength of cementitious materials (FAROOQ et al., 2021; KHAN et al., 2022b; ZHENG et al., 2022). Similarly, the ABR method was also noted to be the best suitable in several studies (AL-HASHEM et al., 2022; ANJUM et al., 2022; SHANG et al., 2022; WANG et al., 2022).

Additionally, k-fold and statistical methods were utilized to evaluate the models' precision. The accuracy of a model increases when the R^2 is high and the degrees of divergence (MAE, RMSE, and MAPE) are minimum. Because the precision of an ML approach is so dependent on the amount of inputs and data samples used to run algorithms (FAROOQ et al., 2021), it is challenging to define and suggest

the best ML technique for prediction in different fields of research. With ensemble ML techniques, the weak learner is used over and over again to build submodels that are trained on the data sample and then fine-tuned to improve accuracy. In this way, the ensemble ML models produce more precise results than any of the individual models could have on their own. The variation in R^2 for the GBR, ABR, and XGB submodels is displayed in Figure 14. For GBR submodels, R^2 varied from 0.762 to 0.781, with a mean of 0.769. The average R^2 for the ABR models was 0.825, with a range of 0.773–0.853. Furthermore, the XGB submodels' R^2 ranged from 0.870 to 0.902, with an average of 0.893. Based on these results, it can be said that the XGB submodels are the most accurate of the three. More specifically, a SHAP analysis was run to learn how various input factors affected the UPV of HFRNSCs and how they interacted with one another. In a greater positive correlation with the UPV of the HFRNSC, specimen age was shown to be a highly useful parameter. The impact of NS on the UPV was also revealed to be more beneficial. It could be relied on by the filler action of NS, which lowers matrix porosity and ultimately raises UPV. However, it was shown that the impact of CA/FA on UPV was more adverse, indicating that a low CA/FA must be maintained to get a higher UPV. Also, it was determined that Vf had both positive and negative effects, suggesting that utilizing Vf up to an optimum amount can improve the UPV, while at larger Vf contents, the UPV may decline. The increasing matrix porosity, which is inversely correlated with matrix porosity (MOHAMMED AND RAHMAN, 2016), may cause decreased UPV at greater CA/FA and Vf. Because of the dearth of alteration in SP/B and w/b in the dataset used, their influence was unclear, and a broader data sample with more inputs and variations might result in better findings.

5 Conclusion

This research aimed to expand the knowledge on how machine learning (ML) models might be used to estimate the ultrasonic pulse velocity (UPV) of hybrid fiber-reinforced concrete modified with nano-silica (HFRNSCs). Three ML methods, including gradient boosting regressor (GBR), adaptive boosting regressor (ABR), and extreme gradient boosting (XGB), were used to evaluate the UPV. Also, SHapley Additive ExPlanations (SHAP) analysis was performed to examine the effect of input features on the UPV of HFRNSCs. The conclusions of this research are as follows:

- Modeling methods showed that the GBR and ABR techniques had a satisfactory level of accuracy with an R^2 of 0.78 and 0.85 for UPV estimation, respectively, while the XGB method had a better level of accuracy with an R^2 of 0.90 for UPV prediction.
- The average difference among actual and estimated UPV (error) in GBR, ABR, and XGB techniques was found to be 0.070, 0.061, and 0.047 km/s, respectively. The error analysis also validated the reasonable accuracy of the GBR and ABR approaches and the superior precision of the XGB model in predicting the UPV of HFRNSCs.
- The SHAP analysis showed that specimen age was a crucial parameter, with a superior positive relationship to the material's UPV. It was also discovered that the effect of nano-silica (NS) on the UPV was more favorable. Nonetheless, it was discovered that the effect of coarse aggregate to fine aggregate ratio (CA/FA) on UPV was more negative, indicating that a low CA/FA must be maintained to increase UPV. In addition, it was revealed that fiber volume (Vf) had both positive and negative impacts, suggesting that incorporating Vf up to the optimal level can increase the UPV; however, at higher Vf concentrations, the UPV may fall.
- The construction sector will benefit from the development of more efficient and cost-effective methods for assessing material properties and the influence of different factors by using novel methods like ML and SHAP analysis.

This study utilized data for which controlled-environment experiments were conducted (laboratory). It is proposed that in future research, actual on-site circumstances, such as humidity, temperature, curing, *etc.*, should be integrated into the modeling phase in order to investigate their effect on the material's strength.

Data availability statement

The original contributions presented in the study are included in the article/supplementary material, further inquiries can be directed to the corresponding author.

Author contributions

KK: conceptualization, methodology, project administration, writing, reviewing, and editing. MA: investigation, resources, writing, reviewing, and editing. US: data acquisition, visualization, writing, reviewing, and editing. WA: conceptualization, software, methodology, validation, investigation, supervision, writing original draft, reviewing, and editing. MF: methodology, resources, writing, reviewing, and editing. AM: data curation, visualization, writing, reviewing, and editing.

Funding

This work was supported by the Deanship of Scientific Research, Vice Presidency for Graduate Studies and Scientific Research, King Faisal University, Saudi Arabia (Project No. GRANT2181).

Acknowledgments

The authors acknowledge the Deanship of Scientific Research, Vice Presidency for Graduate Studies and Scientific Research, King Faisal University, Saudi Arabia (Project No. GRANT2181). The authors extend their appreciation for the financial support that made this study possible.

Conflict of interest

The authors declare that the research was conducted in the absence of any commercial or financial relationships that could be construed as a potential conflict of interest.

Publisher's note

All claims expressed in this article are solely those of the authors and do not necessarily represent those of their affiliated organizations, or those of the publisher, the editors and the reviewers. Any product that may be evaluated in this article, or claim that may be made by its manufacturer, is not guaranteed or endorsed by the publisher.

References

Abirami, R., Vijayan, D. S., John, S. J., Albert, A., and Alex, A. K. (2020). Experimental study on concrete properties using pineapple leaf fiber. *Int. J. Adv. Res. Eng. Technol.* 11 (6), 913–920.

Ahmad, A., Ahmad, W., Aslam, F., and Joyklad, P. (2022). Compressive strength prediction of fly ash-based geopolymer concrete via advanced machine learning techniques. *Case Stud. Constr. Mater.* 16, e00840. doi:10.1016/j.cscm.2021.e00840

Ahmad, A., Chaiyasarn, K., Farooq, F., Ahmad, W., Suparp, S., and Aslam, F. (2021). Compressive strength prediction via gene expression programming (GEP) and artificial neural network (ANN) for concrete containing RCA. *Buildings* 11, 324. doi:10.3390/buildings11080324

Al-Hashem, M. N., Amin, M. N., Ahmad, W., Khan, K., Ahmad, A., Ehsan, S., et al. (2022). Data-driven techniques for evaluating the mechanical strength and raw material effects of steel fiber-reinforced concrete. *Materials* 15, 6928. doi:10.3390/ma15196928

Amin, M. N., Hissan, S., Shahzada, K., Khan, K., and Bibi, T. (2019). Pozzolanic reactivity and the influence of rice husk ash on early-age autogenous shrinkage of concrete. *Front. Mat.* 6, 150. doi:10.3389/fmats.2019.00150

Amin, M. N., Khan, K., Ahmad, W., Javed, M. F., Qureshi, H. J., Saleem, M. U., et al. (2022). Compressive strength estimation of geopolymer composites through novel computational approaches. *Polymers* 14, 2128. doi:10.3390/polym14102128

Amjad, M., Ahmad, I., Ahmad, M., Wróblewski, P., Kamiński, P., and Amjad, U. (2022). Prediction of pile bearing capacity using XGBoost algorithm: Modeling and performance evaluation. *Appl. Sci.* 12, 2126. doi:10.3390/app12042126

Anjum, M., Khan, K., Ahmad, W., Ahmad, A., Amin, M. N., and Nafees, A. (2022). Application of ensemble machine learning methods to estimate the compressive strength of fiber-reinforced nano-silica modified concrete. *Polymers* 14, 3906. doi:10.3390/polym14183906

Ardalan, R. B., Jamshidi, N., Arabameri, H., Joshaghani, A., Mehrinejad, M., and Sharafi, P. (2017). Enhancing the permeability and abrasion resistance of concrete using colloidal nano-SiO2 oxide and spraying nanosilicon practices. *Constr. Build. Mater.* 146, 128–135. doi:10.1016/j.conbuildmat.2017.04.078

Ashrafian, A., Taheri Amiri, M. J., Rezaie-Balf, M., Ozbakkaloglu, T., and Lotfi-Omran, O. (2018). Prediction of compressive strength and ultrasonic pulse velocity of fiber reinforced concrete incorporating nano silica using heuristic regression methods. *Constr. Build. Mater.* 190, 479–494. doi:10.1016/j.conbuildmat.2018.09.047

Aslam, F., Farooq, F., Amin, M. N., Khan, K., Waheed, A., Akbar, A., et al. (2020). Applications of gene expression programming for estimating compressive strength of high-strength concrete. *Adv. Civ. Eng.* 2020, 1–23. doi:10.1155/2020/8850535

Awoyera, P. O., Kirgiz, M. S., Viloria, A., and Ovallos-Gazabon, D. (2020). Estimating strength properties of geopolymer self-compacting concrete using machine learning techniques. *J. Mater. Res. Technol.* 9, 9016–9028. doi:10.1016/j.jmrt.2020.06.008

Bahari, A., Berenjian, J., and Sadeghi-Nik, A. (2016). Modification of portland cement with nano SiC. *Proc. Natl. Acad. Sci. India Sect. A. Phys. Sci.* 86, 323–331. doi:10.1007/s40010-015-0244-y

Barluenga, G., Puentes, J., and Palomar, I. (2015). Early age monitoring of self-compacting concrete with mineral additions. *Constr. Build. Mater.* 77, 66–73. doi:10.1016/j.conbuildmat.2014.12.033

Bolborea, B., Baera, C., Dan, S., Gruin, A., Burduhos-Nergis, D.-D., and Vasile, V. (2021). Concrete compressive strength by means of ultrasonic pulse velocity and moduli of elasticity. *Materials* 14, 7018. doi:10.3390/ma14227018

Cao, M., Khan, M., and Ahmed, S. (2020). Effectiveness of calcium carbonate whisker in cementitious composites. *Period. Polytech. Civ. Eng.* 64, 265. doi:10.3311/ppci.14288

Cao, M., Li, L., and Khan, M. (2018a). Effect of hybrid fibers, calcium carbonate whisker and coarse sand on mechanical properties of cement-based composites. *Mat. construcc.* 68, e156. doi:10.3989/mc.2018.01717

Cao, M., Xie, C., Li, L., and Khan, M. (2018b). The relationship between reinforcing index and flexural parameters of new hybrid fiber reinforced slab. *Comput. Concr. Int. J.* 22, 481–492.

Cao, S., Xue, G., and Yilmaz, E. (2019). Flexural behavior of fiber reinforced cemented tailings backfill under three-point bending. *IEEE Access* 7, 139317–139328. doi:10.1109/access.2019.2943479

Chen, T., and Guestrin, C. X (2016). A scalable tree boosting systemProceedings of the 22nd acm sigkdd international conference on knowledge discovery and data mining. New York, NY. 13 August 2016 New York: Association for Computing Machinery. 785–794. doi:10.1145/2939672.2939785

Chun, B., Kim, S., and Yoo, D.-Y. (2022). Reinforcing effect of surface-modified steel fibers in ultra-high-performance concrete under tension. *Case Stud. Constr. Mater.* 16, e01125. doi:10.1016/j.cscm.2022.e01125

Düğenci, O., Haktanir, T., and Altun, F. (2015). Experimental research for the effect of high temperature on the mechanical properties of steel fiber-reinforced concrete. *Constr. Build. Mater.* 75, 82–88. doi:10.1016/j.conbuildmat.2014.11.005

Erdem, S., Hanbay, S., and Güler, Z. (2018). Micromechanical damage analysis and engineering performance of concrete with colloidal nano-silica and demolished concrete aggregates. *Constr. Build. Mater.* 171, 634–642. doi:10.1016/j.conbuildmat.2018.03.197

Fang, Y., Wang, J., Ma, H., Wang, L., Qian, X., and Qiao, P. (2021). Performance enhancement of silica fume blended mortars using bio-functionalized nano-silica. *Constr. Build. Mater.* 312, 125467. doi:10.1016/j.conbuildmat.2021.125467

Farooq, F., Ahmed, W., Akbar, A., Aslam, F., and Alyousef, R. (2021). Predictive modeling for sustainable high-performance concrete from industrial wastes: A comparison and optimization of models using ensemble learners. *J. Clean. Prod.* 292, 126032. doi:10.1016/j.jclepro.2021.126032

Friedman, J. H. (2001). Greedy function approximation: A gradient boosting machine. *Ann. statistics*, 1189–1232.

Hao, X., Wei, Y., Chen, Z., Zhang, H., Niu, Y., Chen, K., et al. (2021). Mechanical modification of nanomaterials on fully saturated concrete in groundwater reservoir under long-term water immersion. *Front. Mat.* 8. doi:10.3389/fmats.2021.702308

Huang, Q., Gardoni, P., and Hurlebaus, S. (2011). Predicting concrete compressive strength using ultrasonic pulse velocity and rebound number. *ACI Mater. J.* 108.

Huang, Z., Cao, S., and Yilmaz, E. (2021). Investigation on the flexural strength, failure pattern and microstructural characteristics of combined fibers reinforced cemented tailings backfill. *Constr. Build. Mater.* 300, 124005. doi:10.1016/j.conbuildmat.2021.124005

Ilyas, I., Zafar, A., Afzal, M. T., Javed, M. F., Alrowais, R., Althoey, F., et al. (2022). Advanced machine learning modeling approach for prediction of compressive strength of FRP confined concrete using multiphysics genetic expression programming. *Polymers* 14, 1789. doi:10.3390/polym14091789

Karimaei, M., Dabbaghi, F., Dehestani, M., and Rashidi, M. (2021). Estimating compressive strength of concrete containing untreated coal waste aggregates using ultrasonic pulse velocity. *Materials* 14, 647. doi:10.3390/ma14030647

Khan, K., Ahmad, A., Amin, M. N., Ahmad, W., Nazar, S., and Arab, A. M. A. (2022a). Comparative study of experimental and modeling of fly ash-based concrete. *Materials* 15, 3762. doi:10.3390/ma15113762

Khan, K., Ahmad, W., Amin, M. N., Ahmad, A., Nazar, S., and Al-Faiad, M. A. (2022b). Assessment of artificial intelligence strategies to estimate the strength of geopolymer composites and influence of input parameters. *Polymers* 14, 2509. doi:10.3390/polym14122509

Khan, K., Ahmad, W., Amin, M. N., Ahmad, A., Nazar, S., and Alabdullah, A. A. (2022c). Compressive strength estimation of steel-fiber-reinforced concrete and raw material interactions using advanced algorithms. *Polymers* 14, 3065. doi:10.3390/polym14153065

Khan, K., Ahmad, W., Amin, M. N., Aslam, F., Ahmad, A., and Al-Faiad, M. A. (2022d). Comparison of prediction models based on machine learning for the compressive strength estimation of recycled aggregate concrete. *Materials* 15, 3430. doi:10.3390/ma15103430

Khan, K., Ahmad, W., Amin, M. N., and Nazar, S. (2022e1989). Nano-silica-modified concrete: A bibliographic analysis and comprehensive review of material properties. *Nanomaterials* 12, 1989. doi:10.3390/nano12121989

Khan, M., Cao, M., Chaopeng, X., and Ali, M. (2022f). Experimental and analytical study of hybrid fiber reinforced concrete prepared with basalt fiber under high temperature. *Fire Mater.* 46, 205–226. doi:10.1002/fam.2968

Khan, M., Cao, M., Xie, C., and Ali, M. (2022g). Effectiveness of hybrid steel-basalt fiber reinforced concrete under compression. *Case Stud. Constr. Mater.* 16, e00941. doi:10.1016/j.cscm.2022.e00941

Khan, M., Lao, J., and Dai, J.-G. (2022h). Comparative study of advanced computational techniques for estimating the compressive strength of UHPC. *J. Asian Concr. Fed.* 8, 51–68. doi:10.18702/acf.2022.6.8.1.51

Khan, U. A., Jahanzaib, H. M., Khan, M., and Ali, M. (2018). Improving the tensile energy absorption of high strength natural fiber reinforced concrete with fly-ash for bridge girders. *Key Eng. Mat.* 765, 335–342. doi:10.4028/www.scientific.net/kem.765.335

Kou, S.-C., Poon, C.-S., and Wan, H.-W. (2012). Properties of concrete prepared with low-grade recycled aggregates. *Constr. Build. Mater.* 36, 881–889. doi:10.1016/j.conbuildmat.2012.06.060

Latif Al-Mufti, R., and Fried, A. N. (2012). The early age non-destructive testing of concrete made with recycled concrete aggregate. *Constr. Build. Mater.* 37, 379–386. doi:10.1016/j.conbuildmat.2012.07.058

Lencis, U., Udris, A., and Korjakins, A. (2021). Frost influence on the ultrasonic pulse velocity in concrete at early phases of hydration process. *Case Stud. Constr. Mater.* 15, e00614. doi:10.1016/j.cscm.2021.e00614

Li, J., and Deng, Z. (2021). Tensile behavior of hybrid fiber-reinforced ultra-high-performance concrete. *Front. Mat.* 8. doi:10.3389/fmats.2021.769579

Li, Y., Zhang, Q., Kamiński, P., Deifalla, A. F., Sufian, M., Dyczko, A., et al. (2022a). Compressive strength of steel fiber-reinforced concrete employing supervised machine learning techniques. *Materials* 15, 4209. doi:10.3390/ma15124209

Li, Z., Yoon, J., Zhang, R., Rajabipour, F., Srubar, W. V., III, Dabo, I., et al. (2022b). Machine learning in concrete science: Applications, challenges, and best practices. *npj Comput. Mat.* 8, 127. doi:10.1038/s41524-022-00810-x

Mahapatra, C. K., and Barai, S. V. (2019). Temperature impact on residual properties of self-compacting based hybrid fiber reinforced concrete with fly ash and colloidal nano silica. *Constr. Build. Mater.* 198, 120–132. doi:10.1016/j.conbuildmat.2018.11.155

Massana, J., Reyes, E., Bernal, J., León, N., and Sánchez-Espinosa, E. (2018). Influence of nano- and micro-silica additions on the durability of a high-performance self-compacting concrete. *Constr. Build. Mater.* 165, 93–103. doi:10.1016/j.conbuildmat.2017.12.100

Mobini, M. H., Khaloo, A., Hosseini, P., and Esrafili, A. (2015). Mechanical properties of fiber-reinforced high-performance concrete incorporating pyrogenic nanosilica with different surface areas. *Constr. Build. Mater.* 101, 130–140. doi:10.1016/j.conbuildmat.2015.10.032

Mohammed, B. S., Liew, M. S., Alaloul, W. S., Khed, V. C., Hoong, C. Y., and Adamu, M. (2018). Properties of nano-silica modified pervious concrete. *Case Stud. Constr. Mater.* 8, 409–422. doi:10.1016/j.cscm.2018.03.009

Mohammed, T. U., and Rahman, M. N. (2016). Effect of types of aggregate and sand-to-aggregate volume ratio on UPV in concrete. *Constr. Build. Mater.* 125, 832–841. doi:10.1016/j.conbuildmat.2016.08.102

Molero, M., Segura, I., Izquierdo, M. A. G., Fuente, J. V., and Anaya, J. J. (2009). Sand/cement ratio evaluation on mortar using neural networks and ultrasonic transmission inspection. *Ultrasonics* 49, 231–237. doi:10.1016/j.ultras.2008.08.006

Murad, Y. (2021). Compressive strength prediction for concrete modified with nanomaterials. *Case Stud. Constr. Mater.* 15, e00660. doi:10.1016/j.cscm.2021.e00660

Nafees, A., Amin, M. N., Khan, K., Nazir, K., Ali, M., Javed, M. F., et al. (2022a). Modeling of mechanical properties of silica fume-based green concrete using machine learning techniques. *Polymers* 14, 30. doi:10.3390/polym14010030

Nafees, A., Javed, M. F., Khan, S., Nazir, K., Farooq, F., Aslam, F., et al. (2021). Predictive modeling of mechanical properties of silica fume-based green concrete using artificial intelligence approaches: MLPNN, ANFIS, and GEP. *Materials* 14, 7531. doi:10.3390/ma14247531

Nafees, A., Khan, S., Javed, M. F., Alrowais, R., Mohamed, A. M., Mohamed, A., et al. (2022b). Forecasting the mechanical properties of plastic concrete employing experimental data using machine learning algorithms: DT, MLPNN, SVM, and RF. *Polymers* 14, 1583. doi:10.3390/polym14081583

Niewiadomski, P., Stefaniuk, D., and Hoła, J. (2017). Microstructural analysis of self-compacting concrete modified with the addition of nanoparticles. *Procedia Eng.* 172, 776–783. doi:10.1016/j.proeng.2017.02.122

Norhasri, M. S. M., Hamidah, M. S., and Fadzil, A. M. (2017). Applications of using nano material in concrete: A review. *Constr. Build. Mater.* 133, 91–97. doi:10.1016/j.conbuildmat.2016.12.005

Ould Naffa, S., Goueygou, M., Piwakowski, B., and Buyle-Bodin, F. (2002). Detection of chemical damage in concrete using ultrasound. *Ultrasonics* 40, 247–251. doi:10.1016/s0041-624x(02)00146-4

Qi, C., Huang, B., Wu, M., Wang, K., Yang, S., and Li, G. (2022). Concrete strength prediction using different machine learning processes: Effect of slag, fly ash and superplasticizer. *Materials* 15, 5369. doi:10.3390/ma15155369

Qin, D., Gao, P., Aslam, F., Sufian, M., and Alabduljabbar, H. (2022). A comprehensive review on fire damage assessment of reinforced concrete structures. *Case Stud. Constr. Mater.* 16, e00843. doi:10.1016/j.cscm.2021.e00843

Rahmani, E., Dehestani, M., Beygi, M. H. A., Allahyari, H., and Nikbin, I. M. (2013). On the mechanical properties of concrete containing waste PET particles. *Constr. Build. Mater.* 47, 1302–1308. doi:10.1016/j.conbuildmat.2013.06.041

Reches, Y. (2018). Nanoparticles as concrete additives: Review and perspectives. *Constr. Build. Mater.* 175, 483–495. doi:10.1016/j.conbuildmat.2018.04.214

Ren, J., Lai, Y., and Gao, J. (2018). Exploring the influence of SiO2 and TiO2 nanoparticles on the mechanical properties of concrete. *Constr. Build. Mater.* 175, 277–285. doi:10.1016/j.conbuildmat.2018.04.181

Sadeghi Nik, A., and Lotfi Omran, O. (2013). Estimation of compressive strength of self-compacted concrete with fibers consisting nano-SiO2 using ultrasonic pulse velocity. *Constr. Build. Mater.* 44, 654–662. doi:10.1016/j.conbuildmat.2013.03.082

Sadrmomtazi, A., and Fasihi, A. (2010). Influence of polypropylene fibers on the performance of NANO-SIO_2-INCORPORATED mortar. *Iran. J. Sci. Technol. TRANSACTION B- Eng.* 34, 385–395.

Shafabakhsh, G. H., Ani, O. J., and Talebsafa, M. (2015). Artificial neural network modeling (ANN) for predicting rutting performance of nano-modified hot-mix asphalt mixtures containing steel slag aggregates. *Constr. Build. Mater.* 85, 136–143. doi:10.1016/j.conbuildmat.2015.03.060

Shah, H. A., Yuan, Q., Akmal, U., Shah, S. A., Salmi, A., Awad, Y. A., et al. (2022). Application of machine learning techniques for predicting compressive, splitting

tensile, and flexural strengths of concrete with metakaolin. *Materials* 15, 5435. doi:10.3390/ma15155435

Shang, M., Li, H., Ahmad, A., Ahmad, W., Ostrowski, K. A., Aslam, F., et al. (2022). Predicting the mechanical properties of RCA-based concrete using supervised machine learning algorithms. *Materials* 15, 647. doi:10.3390/ma15020647

Sharkawi, A. M., Abd-Elaty, M. A., and Khalifa, O. H. (2018). Synergistic influence of micro-nano silica mixture on durability performance of cementious materials. *Constr. Build. Mater.* 164, 579–588. doi:10.1016/j.conbuildmat.2018.01.013

Sharma, N., Thakur, M. S., Sihag, P., Malik, M. A., Kumar, R., Abbas, M., et al. (2022). Machine learning techniques for evaluating concrete strength with waste marble powder. *Materials* 15, 5811. doi:10.3390/ma15175811

Sufian, M., Ullah, S., Ostrowski, K. A., Ahmad, A., Zia, A., Śliwa-Wieczorek, K., et al. (2021). An experimental and empirical study on the use of waste marble powder in construction material. *Materials* 14, 3829. doi:10.3390/ma14143829

Sukontasukkul, P., Pomchiengpin, W., and Songpiriyakij, S. (2010). Post-crack (or post-peak) flexural response and toughness of fiber reinforced concrete after exposure to high temperature. *Constr. Build. Mater.* 24, 1967–1974. doi:10.1016/j.conbuildmat.2010.04.003

Trtnik, G., Kavčič, F., and Turk, G. (2009). Prediction of concrete strength using ultrasonic pulse velocity and artificial neural networks. *Ultrasonics* 49, 53–60. doi:10.1016/j.ultras.2008.05.001

Wang, C., Xu, S., and Yang, J. (2021). Adaboost algorithm in artificial intelligence for optimizing the IRI prediction accuracy of asphalt concrete pavement. *Sensors* 21, 5682. doi:10.3390/s21175682

Wang, Q., Ahmad, W., Ahmad, A., Aslam, F., Mohamed, A., and Vatin, N. I. (2022). Application of soft computing techniques to predict the strength of geopolymer composites. *Polymers* 14, 1074. doi:10.3390/polym14061074

Wang, X. F., Huang, Y. J., Wu, G. Y., Fang, C., Li, D. W., Han, N. X., et al. (2018). Effect of nano-SiO2 on strength, shrinkage and cracking sensitivity of lightweight aggregate concrete. *Constr. Build. Mater.* 175, 115–125. doi:10.1016/j.conbuildmat.2018.04.113

Xie, C., Cao, M., Guan, J., Liu, Z., and Khan, M. (2021). Improvement of boundary effect model in multi-scale hybrid fibers reinforced cementitious composite and prediction of its structural failure behavior. *Compos. Part B Eng.* 224, 109219. doi:10.1016/j.compositesb.2021.109219

Xu, J., Kong, F., Song, S., Cao, Q., Huang, T., and Cui, Y. (2017). Effect of Fenton pre-oxidation on mobilization of nutrients and efficient subsequent bioremediation of crude oil-contaminated soil. *Chemosphere* 180, 1–10. doi:10.1016/j.chemosphere.2017.03.087

Xue, G., and Yilmaz, E. (2022). Strength, acoustic, and fractal behavior of fiber reinforced cemented tailings backfill subjected to triaxial compression loads. *Constr. Build. Mater.* 338, 127667. doi:10.1016/j.conbuildmat.2022.127667

Xupeng, C., Zhuowen, S., and Jianyong, P. (2021). Study on metakaolin impact on concrete performance of resisting complex ions corrosion. *Front. Mat.* 8. doi:10.3389/fmats.2021.788079

Yan, D., Tian, Y., Liu, K., Chen, S., Zeng, Q., and Ruan, S. (2021). Evaluation of mechanical properties of concrete after exposure to elevated temperatures using ultrasonic pulse velocity measurement and a split-Hopkinson pressure bar. *J. Mat. Civ. Eng.* 33, 04021352. doi:10.1061/(asce)mt.1943-5533.0003983

Yang, D., Zhao, J., Suhail, S. A., Ahmad, W., Kamiński, P., Dyczko, A., et al. (2022). Investigating the ultrasonic pulse velocity of concrete containing waste marble dust and its estimation using artificial intelligence. *Materials* 15, 4311. doi:10.3390/ma15124311

Yao, M., Zhu, Y., Li, J., Wei, H., and He, P. (2019). Research on predicting line loss rate in low voltage distribution network based on gradient boosting decision tree. *Energies* 12, 2522. doi:10.3390/en12132522

Ying, J., Zhou, B., and Xiao, J. (2017). Pore structure and chloride diffusivity of recycled aggregate concrete with nano-SiO2 and nano-TiO2. *Constr. Build. Mater.* 150, 49–55. doi:10.1016/j.conbuildmat.2017.05.168

Yuan, X., Tian, Y., Ahmad, W., Ahmad, A., Usanova, K. I., Mohamed, A. M., et al. (2022). Machine learning prediction models to evaluate the strength of recycled aggregate concrete. *Materials* 15, 2823. doi:10.3390/ma15082823

Zahiri, F., and Eskandari-Naddaf, H. (2019). Optimizing the compressive strength of concrete containing micro-silica, nano-silica, and polypropylene fibers using extreme vertices mixture design. *Front. Struct. Civ. Eng.* 13, 821–830. doi:10.1007/s11709-019-0518-6

Zaid, O., Ahmad, J., Siddique, M. S., and Aslam, F. (2021). Effect of incorporation of rice husk ash instead of cement on the performance of steel fibers reinforced concrete. *Front. Mat.* 8. doi:10.3389/fmats.2021.665625

Zareei, S. A., Ameri, F., Bahrami, N., Shoaei, P., Moosaei, H. R., and Salemi, N. (2019). Performance of sustainable high strength concrete with basic oxygen steel-making (BOS) slag and nano-silica. *J. Build. Eng.* 25, 100791. doi:10.1016/j.jobe.2019.100791

Zhang, N., Yan, C., Li, L., and Khan, M. (2022). Assessment of fiber factor for the fracture toughness of polyethylene fiber reinforced geopolymer. *Constr. Build. Mater.* 319, 126130. doi:10.1016/j.conbuildmat.2021.126130

Zhang, Y., and Aslani, F. (2021). Compressive strength prediction models of lightweight aggregate concretes using ultrasonic pulse velocity. *Constr. Build. Mater.* 292, 123419. doi:10.1016/j.conbuildmat.2021.123419

Zhao, Z., Cao, S., and Yilmaz, E. (2022). Effect of layer thickness on the flexural property and microstructure of 3D-printed rhomboid polymer-reinforced cemented tailing composites. *Int. J. Minerals, Metallurgy Mater.* 30, 1–14.

Zheng, D., Wu, R., Sufian, M., Kahla, N. B., Atig, M., Deifalla, A. F., et al. (2022). Flexural strength prediction of steel fiber-reinforced concrete using artificial intelligence. *Materials* 15, 5194. doi:10.3390/ma15155194